# Stretchable and Flexible Dielectric Loaded RF Coil for MR Images

by

Chavalchart Herabut

A Thesis Presented in Partial Fulfillment
of the Requirements for the Degree
Master of Science

Approved November 2023 by the
Graduate Supervisory Committee:

Sung-Min Sohn, Chair
Rosalind Sadlier
Scott Beeman

ARIZONA STATE UNIVERSITY

December 2023

ABSTRACT

Magnetic resonance imaging (MRI) is the most powerful instrument for imaging anatomical structures. One of the most essential components of the MRI scanner is a radiofrequency (RF) coil. It induces resonant phenomena and receives the resonated RF signal from the body. Then, the signal is computed and reconstructed for MR images. Therefore, improving image quality by increasing the receiver's (Rx) efficiency is always remarkable. This research introduces a flexible and stretchable receive RF coil embedded in a dielectric-loaded material. Recent studies show that the adaptable coil can improve imaging quality by flexing and stretching to fit well with the sample's surface, reducing the spatial distance between the load and the coil. High permittivity dielectric material positioned between the coil and phantom was known to increase the RF field distribution's efficiency significantly. Recent studies integrating the high dielectric material with the coil show a significant improvement in signal-to-noise ratio (SNR), which can improve the overall efficiency of the coil. Previous research also introduced new elastic dielectric material, which shows improvement in uniformity when incorporated with an RF coil. Combining the adaptable RF coil with the elastic dielectric material has the potential to enhance the coil's performance further. The flexible dielectric material's limitations and unknown interaction with the coil pose a challenge. Thus, each component was integrated into a simple loop coil step-by-step, which allowed for experimentation and evaluation of the performance of each part. The mechanical performance was tested manually. The introduced coil is highly flexible and can stretch up to 20% of its original length in one direction. The electrical performance was evaluated in simulations and experiments on a 9.4T MRI scanner compared to conventional RF coils.

# DEDICATION

To all those who have worked tirelessly to advance the field of MRI technology and those who will continue to do so in the future, this message is dedicated to you. Your dedication to truth, knowledge, and progress has led to incredible advancements in medical imaging, and your work has undoubtedly contributed to the betterment of humanity. We continue to push the boundaries of what is possible with MRI technology and always strive to improve the lives of those who rely on it.

ACKNOWLEDGMENTS

I would like to express my sincere gratitude to my family for their unwavering financial and emotional support throughout my academic journey. I would also like to extend my heartfelt thanks to my professor for providing me with this incredible opportunity and for guiding me in the right direction with his/her invaluable insights and research ideas. I am also grateful to my committee members for their helpful suggestions and feedback. I also want to express my gratitude to the MRI scanner center for providing the machine and for their invaluable assistance in solving any scanning issues that arose during my research. Their support was crucial in helping me achieve my research goals. Last but not least, I want to thank my lab members for their endless support and assistance in every area of my life, from work to personal matters. I would not be able to find the trimmer capacitor without their help.

TABLE OF CONTENTS

Page

CHAPTER Page

LIST OF TABLES

LIST OF FIGURES

Figure Page

# CHAPTER 1

## INTRODUCTION

One of the most important advancements in modern medicine has been the development of MRI technology. MRI, or magnetic resonance imaging, is a non-invasive diagnostic tool that uses a powerful magnetic field and radio waves to create detailed images of the body's internal structures. MRI uses the magnetic properties of protons in our bodies to create images. When placed in a magnetic field, the protons align themselves, and a radio frequency pulse is used to disrupt this alignment. As the protons realign, they emit energy that can be detected by a receiver coil and used to create an image.

Focusing on improving the receiver coil for better SNR has been ongoing for over a decade. Studies show that increasing the coil filling factor by positioning the coil as close as possible to the skin's surface shows significant improvement in SNR. Fitting the coil on different patients with different body sizes requires an adjustable coil. Thus, a flexible and stretchable receiver coil is one of the solutions that meets this specification.

Even though putting the coil close to the skin can significantly strengthen the magnetic field, the field rapidly decays as it goes deeper into the body. This suggests the nonuniformity of the field, which means the energy is dissipated on the sample's surface, not an essential part of the interested region, which also saturates the image's contrast. The dielectric material has shown high performance in improving the uniformity of magnets due to the secondary current generated in the dielectric material. This result in a more even distribution of energy; in some case, the field can penetrate deeper into the tissue.

This research addressed the advantages of an adaptable coil combined with dielectric material with a novel design and fabrication technique to produce a flexible and stretchable dielectric-loaded RF coil. The coils were evaluated with EM simulation, bench test, and MRI imaging with a phantom.

The thesis is organized as follows. A brief overview of design potential is described in this introductory chapter. The more in-depth details of related studies and background are described in Chapter 2. The third chapter describes the new design, discussing previous designs and limitations and explaining each research step. Chapter 4 introduces the initial design of the RF coil, including all validation methods used throughout the study. Chapter 5 investigates the stretchable RF coil, focusing on the stretchable conductor component. Significant improvement in the design was described in Chapter 6. Chapter 7 focuses on optimizing the properties and fabrication process of the elastomer dielectric material. The stretchable RF coil and dielectric material were combined and investigated in Chapter 8. Finally, the research findings were discussed and concluded in Chapter 9.

# CHAPTER 2

# LITERATURE REVIEW

## 2.1 Basic of Radio Frequency Coil

Radiofrequency coils are one of the most essential hardware of the MRI scanner. RF coils act like antennae of the scanner, which can transmit and receive MR signals. The transmission coil (Tx) produces a high-power RF pulse perpendicular to the scanner's main magnetic field (B0). This pulse is also considered an electromagnetic B1 field. The coils optimally resonate at the same frequency as the spins of protons inside the human body. To understand this, one must understand the basics of the spins.

All atoms and subatomic particles, including proton, has properties known as spin, which is a fundamental property in nature similar to mass and charge. Under a magnetic field, the spin of the nucleus is known to precess at a specific frequency described by Larmor's equation:

$$f_0 = \gamma B_0$$

Where $f_0$ is the precession frequency, $\gamma$ is the gyromagnetic ratio of the nucleus, and $B_0$ is the applied external magnetic field strength. The gyromagnetic ratio is a quantity that varies depending on the species of nucleus. In MRI, the most common species used is protons since our body contains water, fat, and many other molecules that contain hydrogen atoms, which are only proton nuclei. The gyromagnetic ratio of hydrogen is 42.58 MHz/Tesla. For the 9.4 tesla MRI scanner, the precession frequency is 400.25 MHz, according to Lamor's equation. Hence, the coils must resonate at 400MHz to match with the spins. The resonance frequency of coils used in MRI scanners usually falls in the radiofrequency range, which

is why the coil is called an RF coil. Other than the precession of the spins, they also align themselves with the main B0 field of the scanner. When the B0 field-aligned spins receive the pulse of the B1 field from the transmit RF coil, they are magnetized by the field and flipped to a certain angle depending on the magnitude of RF power of the pulse. The Higher the power results, the more flip angles. When the pulse is absent, the spins relax and gradually realign with the B0 field. During this relaxation, the magnetic precession of the spins produces an RF wave, which is received by a receiver coil. The received RF signal is processed and deconstructed into the MRI image. In some cases, the Tx and Rx coils can be combined, called transceiver coils. This is a very brief description of basic spins, MRI, and coil, which might not be sufficient for the reader unfamiliar with the field. The references provided much more detail regarding these topics. (*Gyromagnetic Ratio (γ) - Questions and Answers in MRI*, n.d.; *Larmor Frequency - Questions and Answers in MRI*, n.d.; *Nuclear Precession - Questions and Answers in MRI*, n.d.; *Spin - Questions and Answers in MRI*, n.d.)

RF coil is an antenna with capacitive and inductive electrical properties due to the nature of the geometry and material of the coil conductor. As a result, the RF has its electrical resonance frequency described with equations:

$$f = \frac{1}{2\pi\sqrt{LC}}$$

Where $f$ is the resonance frequency, $L$ is the coil's inductance, and $C$ is the capacitance of the coil. To maximize the power transfer and minimize the refection power of the coil, the resonance frequency of the coil must match the Lamur frequency by tuning and matching.

The inductor and capacitor can be added to the coil circuit as a matching network to match and tune the coil to the desired frequency.

The most straightforward type of RF coil is a loop coil, which is a conductive wire forming a single loop. This type of coil is usually used as a surface coil. Surface coil placed on area of interest on the surface of the sample. The surface coil is well known for its more localized field and ability to produce a high SNR near the sample's surface close to the coil. However, the coil has a less uniform field pattern with high field intensity near the coil and low intensity deep inside the sample. Multiple surface coils can be added together to form a surface coil array, which can cover more area on the surface.

SNR is one of the most important factors for quantifying the performance of the receiver coil. SNR is defined as a ratio of the mean of signal power to the background noise variation described as:

$$SNR = \frac{\mu}{\sigma}$$

Where $\mu$ is the mean of the signal and $\sigma$ is the standard deviation of the noise. SNR can be affected by many factors, but from a coil design perspective, the factors are coil quality factor (Q) and Filling factor.

The quality factor is a dimensionless value that indicates the loss of the resonator. The definition is the ratio between initially stored and radiated energy per oscillating cycle described as:

$$Q = \frac{Maximum\ Energy\ Stored}{Average\ Energy\ Dissipated\ per\ Cycle} = \frac{\omega L}{R}$$

Where $L$ is the coil's inductance and $R$ is the coil resistance. High coil resistivity results in a low Q value, which is low sensitivity and more susceptible to noise.

The filling factor is the ratio of the magnetic field energy stored inside the sample volume versus the total magnetic energy stored by the loop. Nevertheless, placing a coil that fits closer to the region of interest (ROI) potentially gains better images. (Gruber et al., 2018)

## 2.2 Flexible and Stretchable RF Coil

As mentioned in the previous section, decreasing the distance between the samples increases the filling factor, resulting in an improved SNR. In recent related studies, an adaptable loop coil array prototype was proposed. The design utilizes a stretchable conductive element that allows the coil to stretch and adapt to fit different sizes of patients. Different type of stretchable conductor was experimented with. Amotape (AMOHR, Germany), a commercial stretchable stranded copper wire, is their experiment's most optimal stretchable conductive component. They included the stretchable component in their 6-channel surface coil arrays, allowing the coil to be stretchable in one direction up to 26.68% of its original size. Thus, the coil array can wrap fit to different sizes of samples. The stretchability was also found to shift the resonance frequency of the coil. However, it was easily readjusted using automatic matching and tuning circuitry. The coil was tested compared with a rigid coil on different sizes of phantoms and knee imaging. The coil shows improvement SNR of up to 100% in 20 mm depth. This research shows the superiority of the stretchable coil to the rigid coil. (Gruber et al., 2020)

## 2.3 Dielectric Material for MRI Application

Permittivity is a property of materials that determines the material's ability to store energy when experiencing an external electric field. The field can displace or reorient the atoms or ions in materials, which causes polarization. Under rapid changes in the external electric field, such as RF frequency from the RF coil, the polarization also alternates rapidly, producing a secondary electromagnetic field. The virtual current inside the material is considered a displacement or secondary current. The produced secondary is very useful to combine with the field from the coil to strengthen SNR in specific areas inside the sample. The intensity of the field highly depends on the permittivity of the material. An insufficient permittivity value could result in a faint field. On the other hand, too high permittivity will attract the field very tightly to the material, which cannot penetrate the sample.

For high-field MRI, the high main magnetic field results in a high Larmor frequency, which means the wavelength used in the system is small compared to the body. This causes dark areas near a quarter wavelength in the sample due to the deconstructive interference of the standing wave. Placing high permittivity dielectric pads on the sample's surface can help distribute spatial distribution of the RF fields utilizing the secondary field. The produced fields can fill the void spot. This is said to improve the coil's SNR, homogeneity, and penetration depth. (Ruello & Lattanzi, 2022; Webb, 2011; Yang et al., 2006, 2011)

## 2.4 Dielectric Integrated RF Coil

From the idea of dielectric material, some studies proposed dielectric integrated coil to utilize the secondary electric field generated by the dielectric material to achieve higher coil performance in improving SNR, more localized field, and increasing homogeneity. One study introduced a receiver coil array helmet for brain imaging using high dielectric permittivity material (HPM). Multi-channel coil arrays were integrated on the surface of a head-size high permittivity helmet. Numerical simulations were performed using the proposed eight channels and 30 channels coil array on the high permittivity helmet. The helmet was put on a human head phantom. Eight elements of transmission coils surround the helmet. Multiple permittivity values were tested. The result shows maximum SNR at 100 permittivity. The presence of HPM increases SNR for transmission efficiency average by 55%. The coil helmet was fabricated with the same design as in the 30-channel coil simulation. The HPM was made with ceramic of 107 permittivity, and the images were acquired with a 7T scanner. The HPM coil improves the SNR average by 21%. (Lakshmanan et al., 2021)

Another study proposed a receive-only surface coil array with integrated solid high permittivity material for a 3T scanner. The researcher investigated the HPM on top of the coil instead of filling the space between the coil and the sample. A coil simulation compared the coil without HPM and the coil with HPM on a tissue-like phantom. The coil is modeled as a rectangular loop coil. The result shows a 49% increase in SNR at the measured surface. Next, three rectangular coils were combined into a surface coil array and placed around a cylinder phantom. A birdcage transmission coil surrounded the setup. This

simulation shows an improvement of the transmission coil by 15%. It also shows increases in SNR near the HPM in the phantom by 60%. Later, they replace the phantom with a human voxel body and cover the coil array on the anterior part of the neck. The simulation result shows an increase of SNR near the neck by 20% and small increases of SAR by 2%. The coil array was fabricated and tested in vivo with three subjects. The coils were positioned on the anterior of the neck, and images were acquired. The images show an SNR gain of 52% on average. (Ruytenberg et al., 2020)

In previous studies, dielectric integrated coil designs are rigid, which prevents the coil from fitting close to the sample surface, which wastes some potential gain of SNR. The rigidity also prevents the adaptability to fit all sizes of samples. The solid dielectric material made of ceramic was an obstacle to achieving a flexible RF coil design. Recently, a study investigated flexible and stretchable dielectric material. The introduced dielectric material is elastomer loaded with dielectric ceramic powder. The dielectric powder increases the material's permittivity while having elastic rubber properties. However, this technique still provides a very low permittivity of approximately 10. The material was also used to fabricate RF coils for a 9.4T scanner. The coils were fabricated using copper wire as a circular loop coil. The coils were stabilized in the middle of a mold, and the dielectric-loaded elastomer mixture was poured and cured. Even with a low permittivity value, the resulting image shows an increase in homogeneity. Deeper penetration of the magnetic field in the phantom sample was also observed. Fare artifacts on the phantom closed to the coil conductor were also minimized. However, the proposed coil design still needs to be

more stretchable due to the non-stretchable conductor. (Hashemi, Kandala, & Sohn, 2023; Hashemi, Kandala, Agbo, et al., 2023)

# CHAPTER 3

## RESEARCH DESIGN

This research aims to utilize the adaptability of stretchable and flexible coil design and the performance-enhancing properties of dielectric material. The adaptability could take advantage of reducing the spatial distance between the coil and the sample surface to improve SNR, as experimented in previous studies. The dielectric material has also been shown to improve the coil's efficiency in multiple ways, such as increasing SNR, homogeneity, penetration depth, and small increases of local SAR but decreases in average SAR.

Combining the adaptable RF coil with the dielectric material into a stretchable and flexible dielectric integrated RF coil was hypnotized in this study to enhance the coil's performance even further. However, these enhancing properties depend on many design details and factors of the RF coil and the dielectric material. The flexibility and stretchability also limit the option of dielectric material to elastomer dielectric. The elastomer dielectric-loaded material also has limitations in terms of maximum permittivity. Thus, this study investigated the performance and viability of the stretchable RF coil integrated with dielectric elastomer.

A simple conventional RF loop coil was designed as a basis coil, which can be modified and integrated with other components later in the study. It can also be used as an ideal or a controlled coil for result comparison with the modified coils. As a result, this ideal coil must be validated and optimized using simulation and bench testing for the fabricated coil. Imaging with the scanner is a more complex validation technique that must

be performed, adjusted, and standardized to keep reliability throughout the research. New design, fabrication techniques, and experimenting processes were adjusted along the way to improve the quality of the research.

Next, the stretchable conductive components were investigated and optimized for fabricating the stretchable RF coil. The mechanical and electrical properties of the component must be tested. After fabricating the stretchable RF coil, the coil must be validated at different stretching distances compared with the ideal coil to ensure the functionality of the coil. The added component is expected to have minor effects on the resonance frequency of the coil, the Q factor, and the field pattern of the coil.

The elastic dielectric material was experimented with parallel to the stretchable RF coil. According to previous studies, the optimal dielectric permittivity differs depending on various factors. Thus, the dielectric concentration in the rubber must be tested to find the optimal value. The ideal coils were embedded inside the dielectric material with different concentration values. The images of each coil were acquired with the scanner and analyzed to find the most optimal value. The SNR and field homogeneity improvement were observed. Then, this value was used to fabricate the stretchable dielectric integrated RF coil. The coil must be tested with the scanner to validate the performance at different stretching distances. The electrical properties of the dielectric material are likely to change when stretched due to the increase in length and decrease in thickness. Mechanical stability and flexibility were also observed. With this research process, it should be sufficient to demonstrate the viability of the proposed coil design.

# CHAPTER 4

# RF COIL

The purpose of designing a simple RF coil with no extra function is to be used as an ideal coil mainly for comparing with other presenting coils. It is also an initial design verification to ensure the fundamental design principle and fabrication process. The ideal coil can be modified into more advanced coils by adding more components for more functions.

## 4.1 Design Consideration

The first consideration is that the coil must have a resonance frequency matched with an MRI scanner. This research uses a 17 cm horizontal-bore dry magnet MRI scanner at the Magnetic Resonance Research Center, Arizona State University (MRRC-ASU), to conduct high-field (9.4 T) MR imaging experiments. Thus, with magnet proton spin calculation shown in equation ~~X~~, the resonance frequency must be at 400 MHz. Thus, the inductance of the coil and the adding breaking capacitors must be calculated to incorporate this frequency. The coil size must be small enough to be inserted inside the scanner bore, including phantom and other fixate equipment. The coil also needs enough space for a matching circuit and connection port for the coaxial cable to connect to the scanner console. The coils should also be able to scale into more than one channel for future testing. For the ability to be modified for stretchability, the coil is designed to have stretchability in one direction sufficient to demonstrate the stretching performance. The stretchable conductor components must allow the coil to stretch in one direction. The dielectric material is also able to be integrated with the coil.

According to these initial specifications, the coil's geometry should be a rectangle, which allows stretchable conductors to be included on two parallel sides and the matching circuit and distributive capacitor on the two other sides of the rectangle coil. A simple diagram of the coil is shown in Figure 1 below. This design limited the distributive capacitors to a maximum of one due to the space limitation. The capacitor value range is one of the main limitations of the coil design. The minimum practical value is 1pF. Hence, the coil self-inductance must be low enough to maintain the resonance frequency at 400MHz. When the stretchable conductors and dielectric material were integrated with the coil, including the loading effect from the phantom, this increased the inductance and/or capacitance, resulting in lower resonance frequency. Even with the network matching circuit, the tunability range is limited to the required practical capacitor values. Due to this challenge, the size and geometry must be carefully selected for all practical tunability ranges.

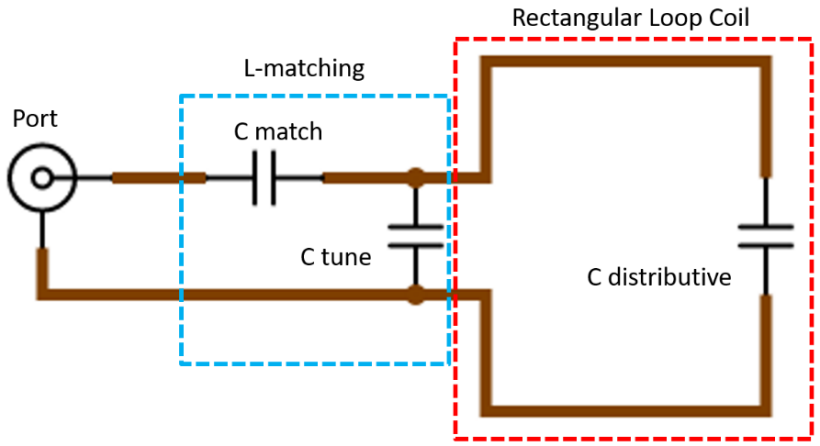


Figure 1. Diagram of the Conventional Coil

The initial size of the coil was selected by estimating the self-inductance of the coil using equation:

$$L_{rect} \approx N^2 \frac{\mu_0 \mu_r}{\pi} \left[ -2(W+h) + 2\sqrt{h^2+W^2} - h \ln\left(\frac{h+\sqrt{h^2+W^2}}{W}\right) \right.$$
$$\left. - W \ln\left(\frac{W+\sqrt{h^2+W^2}}{h}\right) + h \ln\left(\frac{2h}{a}\right) + W \ln\left(\frac{2W}{a}\right) \right]$$

Where $N$ is the number of turns, $W$ is the width of the rectangle in meter, $h$ is the height or the rectangle in meter, $a$ is the wire radius $\mu_r$ is the relative permeability of the medium, and $L_{rect}$ is the result inductance in henry. (*Inductance of Rectangular Loop · Technick.Net*, n.d.)

Then, inductance was used to estimate the required value of the capacitor using a coil development tool. (*Coil Development Calculator - Single Loop Resonator Surface Coil*, n.d.) With a rectangle loop coil with a base size of 30 mm in length and width, the coil has approximately 75.3 nH, which required breaking capacitor values of 2.103 pF. This leaves some room for tunability. Assuming the coil is stretched to 1.5 times the original length, the inductance increases to 99.71 nH, which requires a capacitance of 1.588 pF. This value remains in the practical range and also leaves some tolerance for including stretching elements and loads. Furthermore, 30 mm. in size allows more than one coil to be inserted inside for multi-channel purposes, leaving some room for stretching and matching circuits and connectors.

## 4.2 EM Simulation

Commercial electromagnetic simulation Ansys HFSS was used to optimize the coil design further. The coil conductor is a copper sheet with a width of 3mm, forming a rectangular loop. The loop coil has a width of 30mm and a length of 30mm. The conner has 45-degree bends to minimize parasitic capacitance. The far side of the coil has a serial lumped RLC boundary condition component representing a distributive capacitor. The near side of the coil also has serial and parallel lumped RLC as a matching and tuning capacitor, forming an L-matching network. The matching network is then connected to a coaxial cable. The cable's far end is excited using a terminal wave port with 1 watts of power. The coil is placed on a 100 x 100 x 60 mm cuboid phantom. The geometry setup of the simulation is illustrated in Figure 2. The material of the phantom is edited to imitate muscle tissue at 400MHz. The muscle has a relative permittivity of 57.13, conductivity of 0.8 S/m, and loss tangent of 0.63. The radiation box surrounded the models with a minimum of 150 mm from each side of the model. The S-parameter and magnetic field inside the phantom were then used to optimize the coil's capacitor value and minor geometry. The S11 shows good resonating, and the magnetic field plot shows a deep and intense magnetic field inside the phantom. The result S11 shows well resonating at 400MHz. The result magnetic field plotted in Figure 3 shows a typical field pattern inside the phantom. This indicates that the design can function as intended.

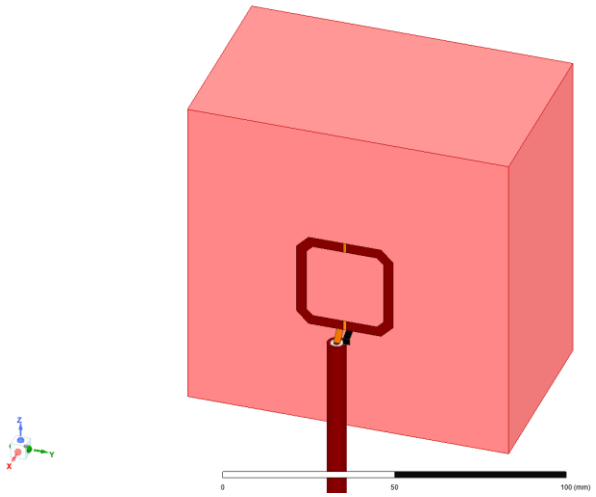


Figure 2. Conventional Rectangle Loop Coil Simulation Setup

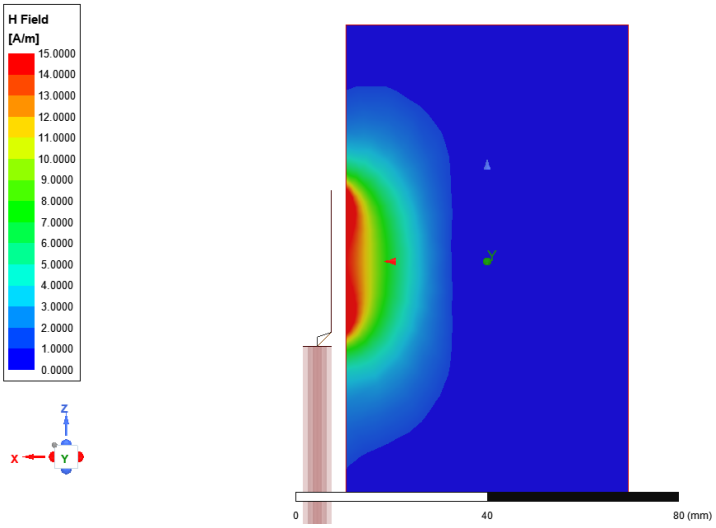


Figure 3. Simulated Magnetic Field of Conventional Rectangle Loop Coil

## 4.3 Coil Fabrication

Copper tape with a width of 3mm was used as the conductive part of the loop coil. The loop coil has a length and width of 30 mm. The tape was attached to a thin 3D-printed piece for mechanical support. The corners of the loop are folded as 45-degree bends. A small non-magnetic trimming capacitor was soldered on the far side of the coil as a distributive capacitor. The other side was soldered to an L-matching circuit board, which was hot glued to the 3D printed piece. 2 trimming capacitors are used as the matching and tuning capacitors. Due to the space limitation in the scanner bore, a cut coaxial cable was used as the connector instead of the usual RF connector. The fabricated coil is shown in Figure 4 below.

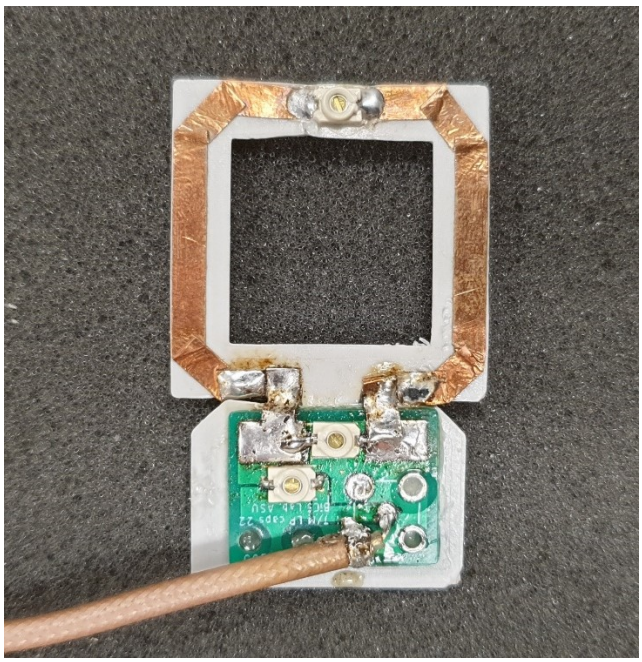

Figure 4. Fabricated Ideal RF Coil

A muscle phantom solution was prepared for bench testing and imaging. The electrical properties are similar to the one used in the EM simulation of muscle at 400MHz. The dielectric constant of 57.13 and conductivity of 0.8 S/m were used to calculate the amount of water, sugar, and salt. For 116 g of water, sugar is 113 g, and salt is 4 g. All ingredients were mixed using a mixer until all sugar dissolved into the water. Then, the solution was sealed in a plastic bottle, ready to be used, as shown in Figure 5 below.

Figure 5. Phantom Solution Bottle

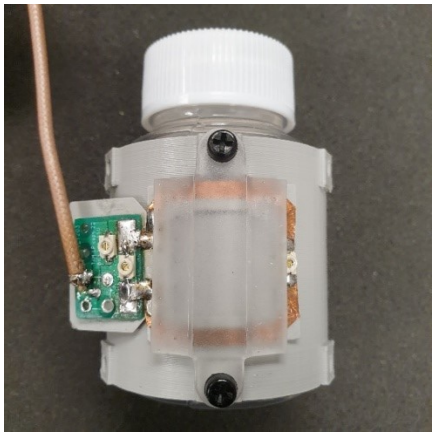

Figure 6. RF Coil Fixed on the Phantom

The coil was fixed on the phantom with a simple 3D-printed structure, as shown in Figure 6. For bench testing, the coil was connected to the vector network analyzer (VNA) to measure the reflection coefficient and determine the resonance frequency. The coil was tuned and matched to resonate slightly lower than 400MHz to compensate for the inductive coupling of the MRI scanner bore.

### 4.4 Image Acquisition

The setup was inserted in the MRI scanner mentioned in section 4.1, which is shown in Figure 7 below. The coil was well matched and tuned to resonate at 400MHz with S11 below -15dB inside the bore. The B0 field was adjected for uniformity through shimming to reach 10000. For the MR imaging protocol, according to the previous literature for flexible dielectric material, a Fast-Low-Angle-Shot (FLASH) Sequence was used. The imaging parameters were set to a repetition time (TR) of 100 ms, an echo time (TE) of 4 ms, and a flip angle (α) of 25°. The field-of-view (FOV) was set to 60 × 60 mm with a matrix size of 256 × 256, resulting in an in-plane resolution of 234 × 234 μm. Eight 1 mm slices were taken from the sample with a 0.2 mm gap between them, similar to the literature. The first resulting image in Figure 8 below shows a typical magnetic field pattern inside the phantom. Some visible artifacts and noise might result from an imperfect fabrication process. Thus, some processes were redone and adjusted later in the study.

Figure 7. Dry Magnet MRI Scanner (9.4T)

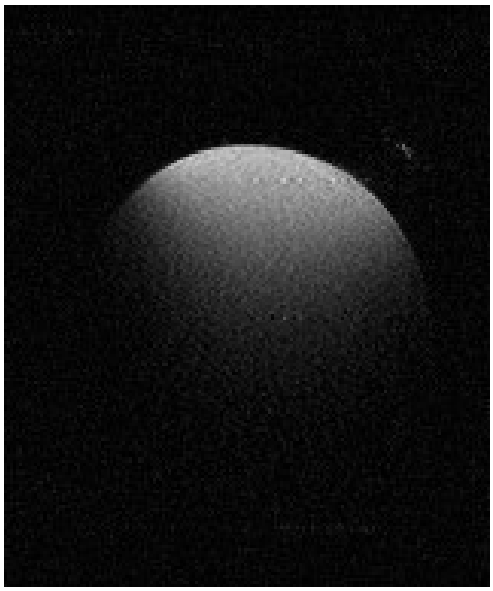

Figure 8. Acquired MRI Image of Ideal Coil

# CHAPTER 5

# STRETCHABLE RF COIL

In this section, the stretchable conductor, the core component of the stretchable coil, was designed referencing the literature. The design was optimized, and the electrical and mechanical capabilities were measured. The conductor was later combined with the ideal coil into a stretchable coil. Then, the performance of the coil was evaluated at different stretching lengths.

## 5.1 Stretchable Conductor

According to stretchable conductor experiments from the adaptable coil literature, Amotape performs best in their stretchable conductor comparison experiments. The conductor is a commercial stretchable 2D wave pattern copper wire integrated with three elastic strings along the length of the wire. The elastic strings produce the return force to return the wire to its original shape evenly after being stretched.

For this research, Amotape was simplified into a simple, thin copper wire with similar 2D wave patterns. Since the conductor was planned to be embedded inside elastic material later in the study, the material can provide the return force. Thus, the elastic strings are not necessary. The wave pattern of the conductor also highly affects the performance of the conductors. The wave number of the pattern along the length of the wire affects its stretching length. More waves allow the conductor to stretch more but also result in challenging fabrication and might introduce too much inductance and capacitance to the coil, reducing the RF coil's tunability and magnetic field pattern. The diameter of the copper wire also affects the mechanical and electrical properties of the conductors.

However, the copper wire is cheap and easy to fabricate and test. Hence, the optimal wave numbers and the thickness of the copper wire were achieved through multiple iterations of trial and error.

### 5.1.1 Fabrication

Different copper wire sizes were manually cut and bent into wave pattern shapes. The size of the conductor piece must fit with the designed ideal RF coil, resulting in a total length of 24 mm and width of approximately 3-4 mm. The wire's thickness highly impacts the ability to be shaped into a wave pattern. After some trial and error, wires bigger than 0.5 mm in diameter are too rigid to bend and provide no ability to be stretched. A 0.5 mm wire was selected in this research.

The copper wire was cut and shaped into a spring pattern by compressing the wire between 3D-printed spring molds. The molds implement the wave pattern of the sine function. The molds were printed and tested by compressing the wire in between. When the number of waves is high, it is hard to compress the wire into the wave pattern, and it usually breaks the wire in the middle due to too much strain. However, the piece allows very small stretchability when the wave number is too low. Thus, the wave numbers were optimized to 3.5. The optimized fabrication process is illustrated in Figure 9.

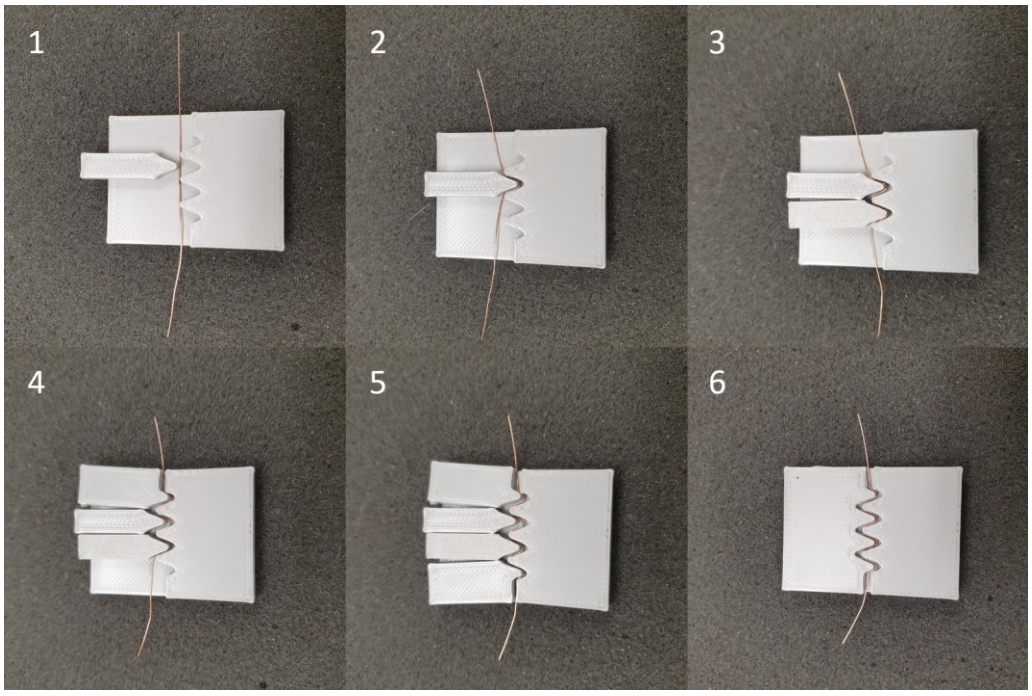


Figure 9. Stretchable Conductor Component Fabrication Process

### 5.1.2 Elastic Material Embedded Conductor

The stretchable conductor cannot return to its original shape due to the lack of return force. Since the coil is designed to be integrated with a flexible elastic dielectric material, the return force of the elastic material might be utilized as the wire-returning mechanism when the wire is embedded inside the elastic material. To verify the idea, the conductors were embedded in elastic dielectric material. The material mixture consists of silicone rubber Ecoflex (Smooth-On, USA) 30 parts A and B with a ratio of 1:1 by weight. The mixture was carefully mixed until uniform. A 3D-printed mold was made to case the rubber around the conductor, as shown in Figure 10. The conductor was fixed in the middle of the mold, and then the mixture was poured into the mold and waited to be cured. After more than 4 hours of curing, the elastic conductor piece was removed from the mold and ready to be tested, as shown in Figure 11.

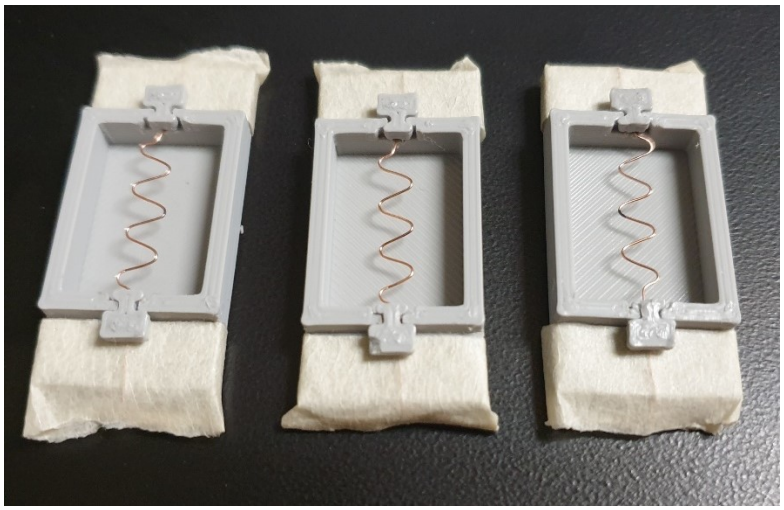

Figure 10. 3D-printed Mold for the Stretchable Conductors

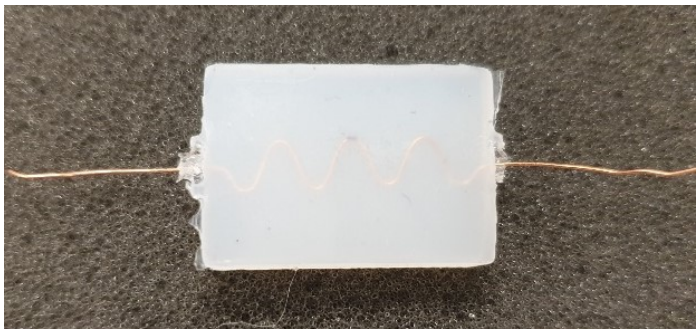

Figure 11. Elastically Stretchable Conductor

### 5.1.3 Mechanical Stretchability

The elastic conductor must be able to stretch to a certain length and return to its original shape without deforming or breaking the wire. Since the silicone is translucent, the wave pattern conductor can be observed easily. The conductor was stretched by hand multiple times to different distances to find a distance that deformed the conductive wire, as shown in Figure 12. After many trials, the conductor can be stretched at approximately 25% stretchability of its original length.

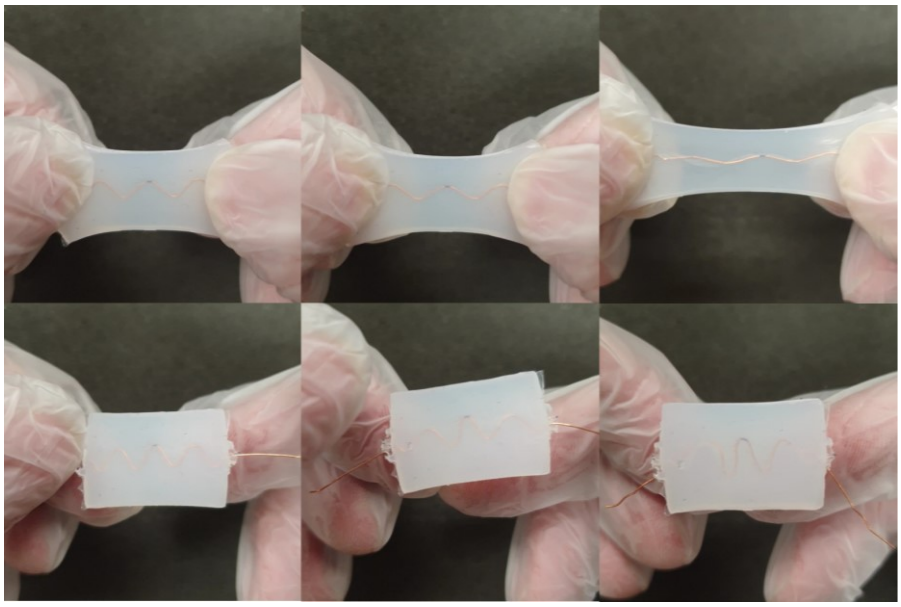

Figure 12. The Stretchable Conductors Stretch Testing

### 5.1.4 Electrical Properties

When a copper wire changes in geometry, its electrical properties, especially the inductance, alter. The properties highly affect its resonance frequency and will highly affect the resonance frequency of the RF coil when integrated into the coil. Thus, the inductance of the stretchable conductor was measured to measure the magnitude of change, which determines the tunability of the coils.

Three stretchable conductors were stretched to 3 different distances: 24mm, 26mm, and 29mm. The 24 is the length of the original shape of the spring. The spring is then fixed with glue on a plastic piece for stable measurement. A simple 3mm width copper tape with 24mm length was also measured as a perfect conductor for comparison. Then, each piece was measured with an RLC meter at 1MHz, the maximum frequency the machine is capable of. The inductance result is shown in Table 1. The result shows a slightly different

value, which is not significant. However, the accurate change must be measured again when added to the RF coil.

Table 1. Electrical Properties of Stretchable Conductors

| Conductor | Length (mm) | L (uH) |
|---|---|---|
| Copper Tape | 24 | 2.739 |
| Patterned Copper Wire | 24 | 2.035 |
| Patterned Copper Wire | 27 | 2.034 |
| Patterned Copper Wire | 30 | 2.008 |

## 5.2 RF Coil Integrated with Wave Pattern Conductor

### 5.2.1 EM Simulation

The conventional coil simulation in the previous simulation section was modified. Two wave pattern conductors replaced both sides of the RF coil, as shown in Figure 13 below. This coil configuration is called a stretchable coil in this research. The conductors were modeled as a copper sheet with sine wave patterns with a width of 1 mm. The stretchable coil is also stretched from 30 mm. in length to 36 mm. to simulate the effect of stretching the conductor on the tunability and the magnetic field. This stretched the stretchable conductor by 6 mm. similar to the experiment in the previous section. A pair of conventional coils with lengths of 30 mm. and 36 mm. were also simulated for comparison. The simulation setup is similar to the RF coil simulation in the previous chapter.

In Figure 14, plots a1 and a2 are magnetic field magnitude inside the phantom of the ideal coil simulations with the length of 30 mm. and 36 mm. in order. The plots b1 and b2 are of the stretchable coil of 30 mm. and 36 mm. in length. The magnetic field result shows a decrease in intensity inside the phantom of the stretchable coils compared to the ideal coils simulation for both stretching lengths. This might be a trade between the stretchability and magnetic field intensity. However, the SNR is expected to increase in the practical setting because the flexible and stretchable coil could fit more on the surface than the rigid, non-stretchable counterpart, increasing the filling factor.

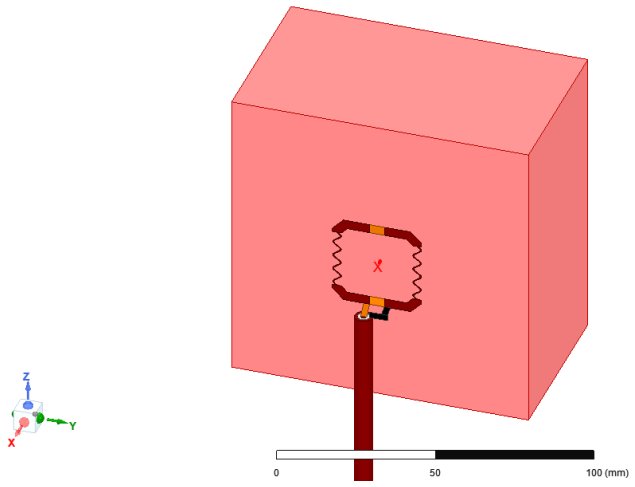


Figure 13. Stretchable Rectangle Loop Coil Simulation Setup

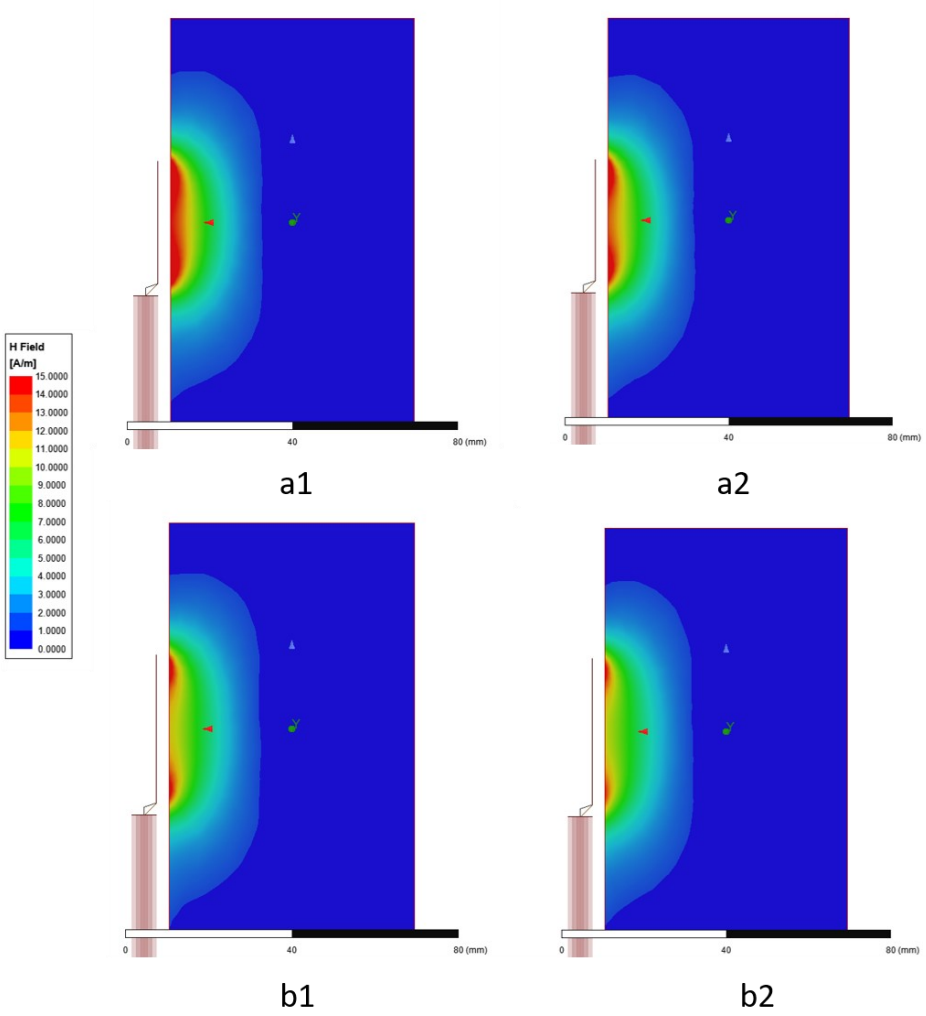


Figure 14. Simulated Magnetic Field of the Ideal Coil and Stretchable Coil

### 5.2.2 Fabrication

The coil is fabricated similarly to the conventional coil in the previous chapter, using copper tape as the conductor. However, the copper tape on the side of the coil was replaced with the wave pattern conductor soldered to the tape. Three coils were made and stretched to three different stretching distances to test the effect of stretching distances of the stretchable coil. Due to the original length of the stretchable conductor of 24 mm and the maximum stretching length of 30 mm, adding the width of the conductor, the length of the coil is 30 mm, 33 mm, and 36mm, which can be interpreted as 0%, 10% and 20% of stretching in length. The 3D-printed support structure underneath the coil also has the length following the coil length. Figure 15 below shows all three fabricated coils. Testing with VNA shows that adding the stretching component lowers the resonance frequency. Stretching the coil also lowers the resonance frequency as well. However, the trimmer capacitors can tune the resonance frequency back to 400 MHz.

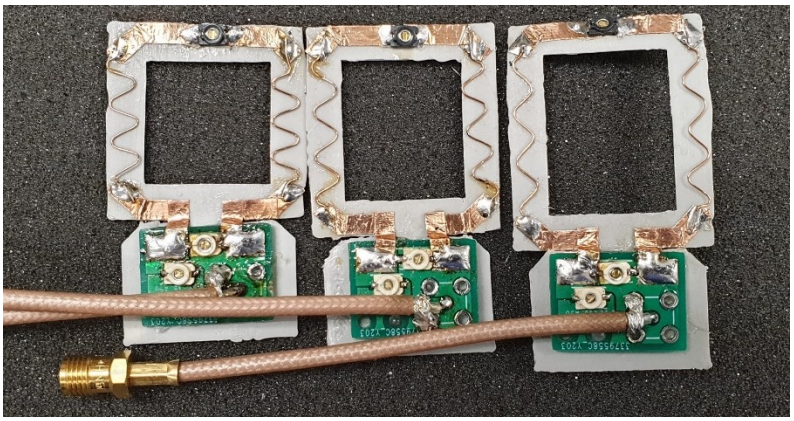

Figure 15. Stretchable Conductor RF Coils of 0%, 10%, and 20% Stretching Lengths

The stretchable conductor coils were compared with a set of ideal coils with the corresponding length shown in Figure 16 to observe the effect of adding the stretchable conductor. The introduced coil sets are expected to perform slightly inferior to the conventional coil in the magnetic field intensity, similar to the simulation.

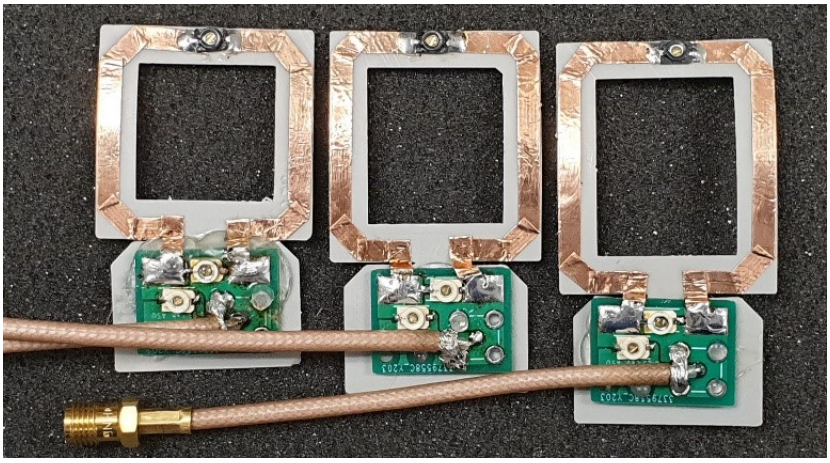

Figure 16. Ideal RF Coils Imitate 0%, 10%, and 20% Stretching Lengths

### 5.2.3 Image Acquisition

Three images of the ideal coils set and three images of the stretchable coils set were acquired using the same scanner with the same setting and protocol as the previous chapter. All coils were well-tuned to resonate at 400MHz and have S11 below -15dB. The shimming level of each coil was also adjusted to approximately the same level. All factors were controlled to keep reliability between each image.

In Figure 17 below, images in the top row from left to right are the ideal coils with 0%, 10%, and 20% stretching lengths in order. Images in the bottom row from left to right are the stretchable coils with 0%, 10%, and 20% stretching length in order. Overall, the images contain a significant amount of background noises and artifacts. Images of the ideal

coil at 0% and 10% have very different noise and magnetic field intensity levels. This indicates high inconsistencies in the experiment. Poor manual coils fabrication process might introduce some conductor discontinuity problems from the folding of copper tape, which includes certain levels of parasitic inductance and capacitance. Performing imaging with a custom RF coil is a complicated process requiring a deep understanding of the MRI scanner and many hours of practice. The lack of experience might also be the source of the inconsistency. The technical issue must be addressed to acquire the true result before progressing to the next step.

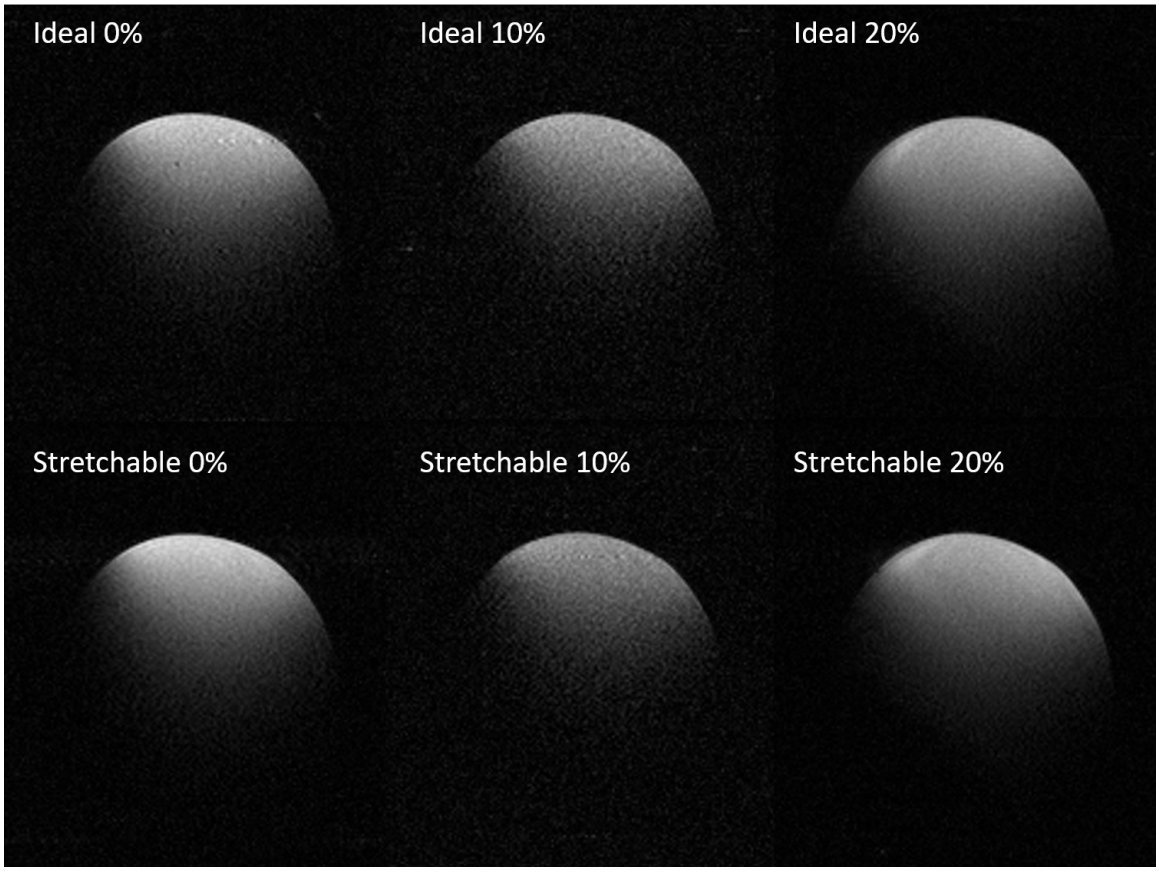


Figure 17. MRI Images Result of Ideal Coils and Stretchable Coils

# CHAPTER 6

# PCB RF COIL

The coil fabrication process and imaging protocol were inspected to reduce the possible cause of the inconsistency issue from the end of the previous chapter. This chapter eliminated and replaced the handmade coils with printed circuit board (PCB) RF coils. PCB ideal coils and stretchable coils are designed and fabricated. The imaging protocol was also optimized to improve the consistency. The images of the coils are acquired and compared.

## 6.1 Design and Fabrication

The ideal coils were designed with KiCad, an electronic design automation software. The geometry of the coil is similar to the previous design. The width of the copper trace of the loop coil is 3 mm. The width of the loop coil is 30mm. 45-degree bends are included at the corners of the loop to mitigate possible parasitic capacitance. Furthermore, the L-matching network was also integrated with the loop coil in the same PCB. The design in the software is illustrated in Figure 18. Similar to the previous chapter, three versions of the coil were made with three different lengths of 30, 33, and 36 mm. for the comparison purpose with the stretching lengths 0%, 10%, and 20% of the stretchable coils.

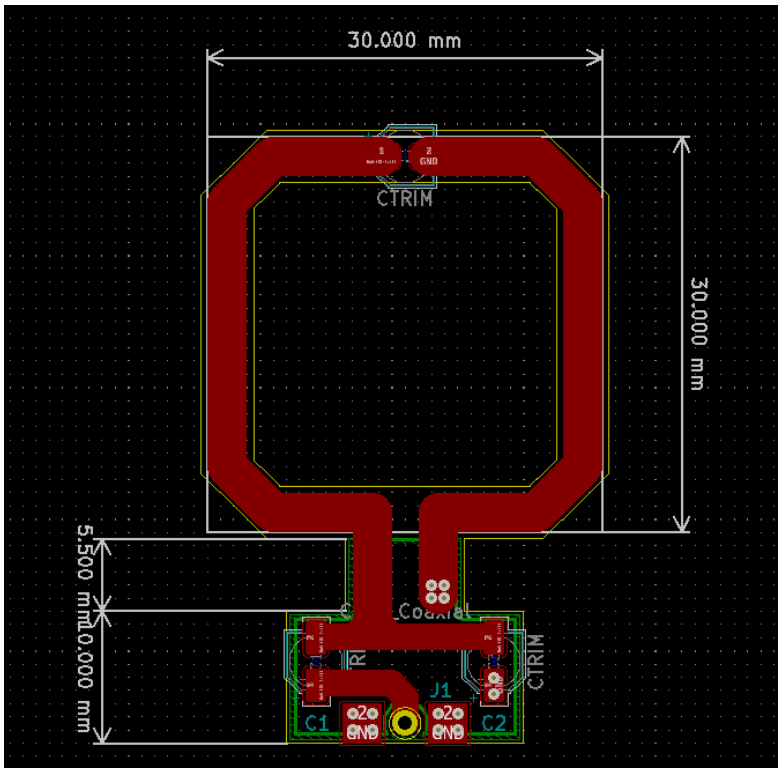


Figure 18. Ideal Coil Design in KiCad

For the stretchable coil, the ideal PCB was altered. The side conductor lines were removed, which split the PCB into two pieces. Both pieces have solder pads for the stretchable conductors to be soldered and join both pieces together to form a loop coil. Figure 19 shows a PCB containing 2 top pieces of the coil. The PCB can be cut to split into two pieces. Figure 20 show the bottom piece of the coil.

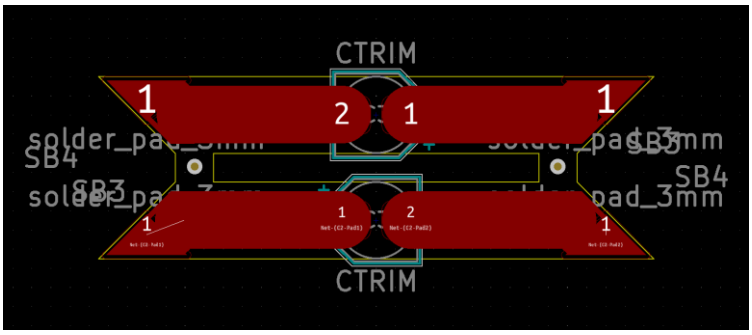


Figure 19. Top Parts of Stretchable Coil PCB

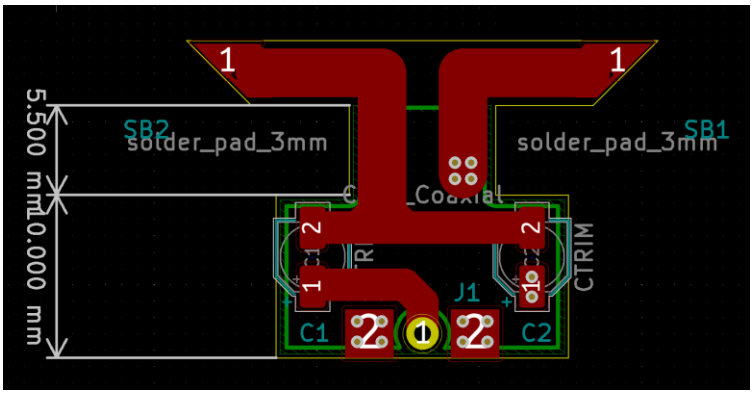


Figure 20. Bottom Parts of Stretchable Coil PCB

All PCBs were manufactured by JLCPCB (Guangdong, China). The manufacturer provides high-quality PCB fabrication at cost-efficient prices, even in low quantities, which is very suitable for our situation. The PCBs were ordered as two layers with 1oz copper caddling for both layers. The substrate is FR4, with a thickness of 0.6 mm. The thickness is minimized to reduce the effect of permittivity of the substrate. The PCBs were soldered manually in our lab. The ideal PCB RF coil is shown in Figure 21. Moreover, the stretchable PCB RF coil is shown in Figure 22.

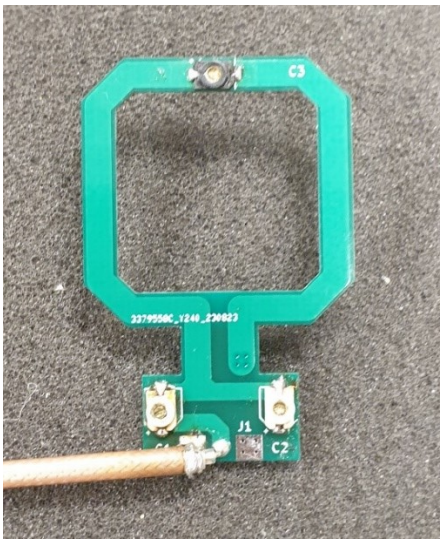


Figure 21. Ideal PCB RF Coil

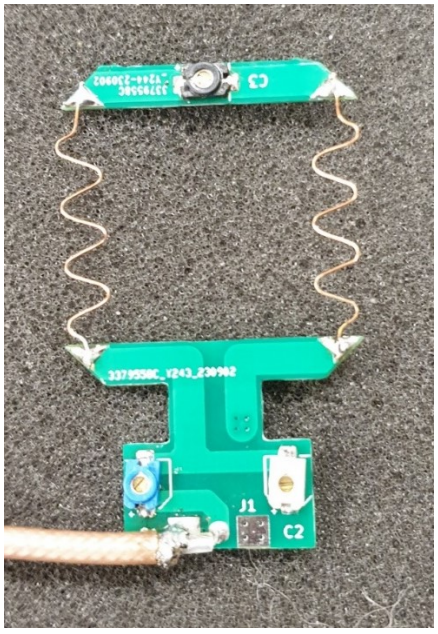


Figure 22. Stretchable PCB RF Coil

## 6.2 Bench Testing

Specific tests on the bench were performed to validate the coils. The coils were matched and tuned with the phantom solution to resonate below -20dB at 400 MHz using the VNA. All the coils can resonate well with approximately a high Q factor. Even though the S11 plot shows good resonating, the main resonating component might not be the loop coil but other components, such as the matching network. A magnetic field probe was used to measure the near magnetic field around the coil to evaluate the coil further. The probe was connected to the second port of the VNA, and the S21 was plotted. S21 indicates the RF power from port 1 to port two or, in this case, from the RF loop coil to the magnetic field probe. A high level of S21 means high power from the coil transfer to the magnetic probe in terms of magnetic field radiation. The S21 of the coil was measured when the probe was positioned at three different locations: on top of the loop coil, on the side of the loop coil, and top of the matching network, as shown in Figure 23 below. The results S21 are -5dB, -16dB, and -19 dB in order. The higher S21 when the probe was positioned atop the loop conductor indicates that it is the main resonating component. This verifies the functionality of the coil.

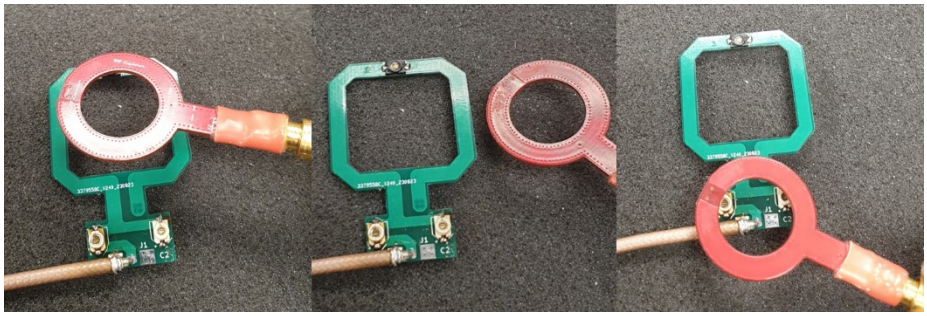

Figure 23. RF Coil 3 Positions Magnetic Field Measurement

## 6.3 Image Acquisition

The three sizes of the ideal coils were stabilized on a 3D-printed structure that snaps fit with the phantom solution bottle. Three stretchable coils were made. Each coil was stretched to 3 different stretching lengths referred to as 0%, 10%, and 20% of the original length. They were glued on a 3D-printed structure similar to the ideal coils set. Figure 24 shows both coils set side by side.

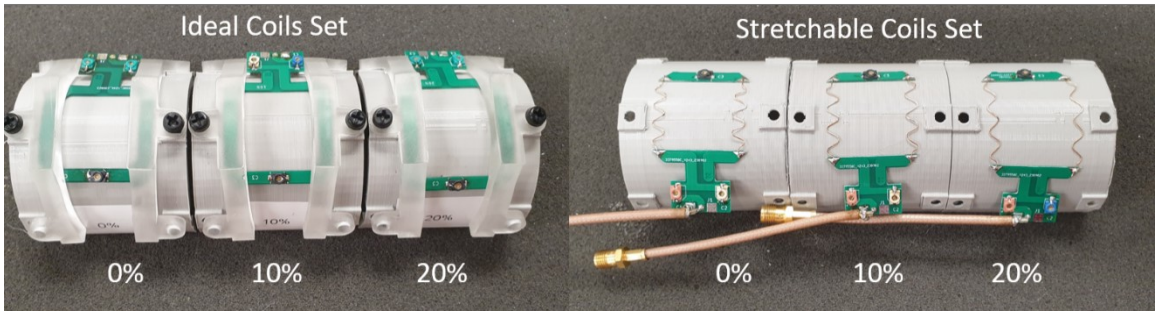


Figure 24. PCB Ideal Coils Set and PCB Stretchable Coils Set

The image acquisition of each coil was performed with the same 9.4T MRI scanner. However, the protocol parameters were slightly adjusted to increase the signal and reduce the noise. The imaging parameters were changed to TR of 100 ms., TE of 5 ms., and α of 50°. Figure 25 shows the result image comparison of each coil. The top row from left to right is the ideal coils with 0%, 10%, and 20% stretching lengths in order. Images in the bottom row from left to right are the stretchable coils with 0%, 10%, and 20% stretching length in order. Two ROIs were placed on each image to measure the average intensity inside that ROI. These values were divided by the standard deviation of the background noise to calculate SNR inside each ROI. At 0% stretching, the SNR near the surface of the stretchable coil significantly drops from 55.51 to 38.7. As the stretchable coil was

stretched, the SNR of that area slowly increased to match the ideal coil of the same length. The decrease might be the result of the wave pattern of the conductor. As the conductor becomes straighter from stretching, the effect is reduced. This behavior was also predicted with the simulation in section 5.2.1. No significant change was observed in the SNRs of the deeper ROI.

Even though the conductor might degrade the field near the surface, it might be compensated by the secondary field generated by integrating dielectric material.

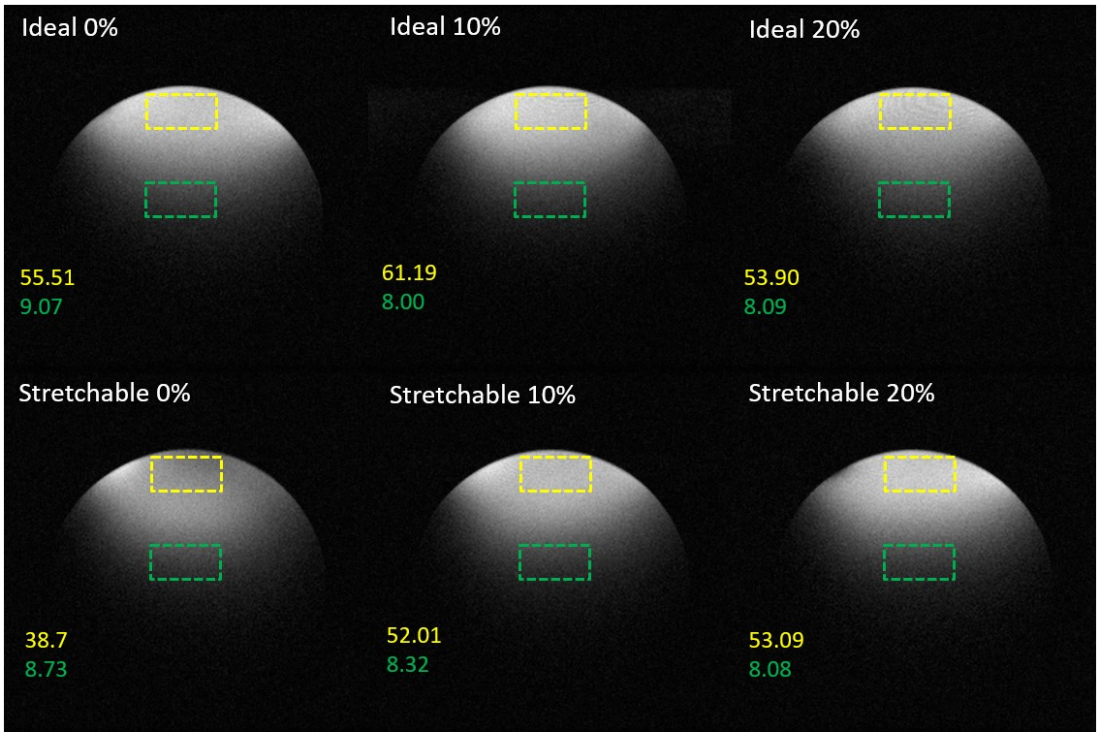


Figure 25. MRI Images Result of PCB Ideal Coils and Stretchable Coils

# CHAPTER 7

# FLEXIBLE DIELECTRIC INTEGRATED RF COIL

From many related studies, the dielectric material's permittivity depends on numerous factors that are hardly predictable. Thus, experimenting for the optimal value is required. In this section, 3 RF coils integrated with flexible dielectric material with three different dielectric power concentrations were tested and compared.

## 7.1 Fabrication

The dielectric material must have elastic properties to achieve flexibility and stretchability. The material should also be able to be shaped into a designed shape. Thus, curable elastic silicone rubber EcoFlex was chosen as the main structural ingredient. (Hashemi, Kandala, Agbo, et al., 2023) The EcoFlex parts A and B were mixed manually with a ratio of 1:1 in weight. Silicon carbide (SiC) powder was added to the mixture to increase the dielectric properties of the elastic material. The mixture was mixed thoroughly. The concentration of the SiC was varied to observe the effect of the concentration of dielectric material. Three ratios of SiC to the EcoFlex mixture by weight were experimented with: 1:6, 1:2, and 1:1.

The ideal RF coils were integrated into the dielectric material. A 3D-printed mold was designed to stabilize the RF coil in the middle of the dielectric material. After that, the dielectric mixture was poured into the mold embedded in the RF coil inside. Then, the molds were placed in a vacuum tank to minimize air bubbles. The mixture was left to cure for at least 4 hours before being removed from the mold. Figure 26 below shows the fabrication process of the coils. The dielectric material on the distributive capacitor solder

pad was manually removed to be able to solder the capacitor. After soldering the capacitor for the matching network, the coils are ready to be used.

Figure 26. Dielectric Integrated Coils Fabrication Process

On the bench test, the coil was tuned to resonate at 400 MHz. Due to the higher dielectric loading effect of a high dielectric constant, the coils tend to resonate at lower frequencies. They can be easily adjusted by matching and tuning the resonance frequency to 400 MHz. In some cases, the coil cannot be turned back with the current range of the trimmer capacitor; the capacitor may be replaced with a fixed capacitor with lower capacitance. The coil's magnetic field was also observed using a magnetic field probe. This observation ensures that the resonating element is the dielectric-loaded loop coil, not the matching network.

## 7.2 Image Acquisition

Due to the rigidity of the PBC RF coil embedding inside a soft and elastic material, it is impractical to bend the coil around the cylinder phantom. Thus, the phantom was replaced with the cuboid phantom. The dielectric integrated coils were placed on top of the phantom and secured with 3D-printed pieces and tape. The ideal RF coils were also used to acquire the images with that same phantom to compare the result.

Figure 27 shows the result image comparison. The image on the top left is the ideal coil. The image on the top right is the dielectric-loaded coil with a 15% dielectric concentration. Images on the bottom row from left to right are the dielectric-loaded coil with 33% and 50% dielectric concentration in order. 2 ROIs were placed to measure the SNR.

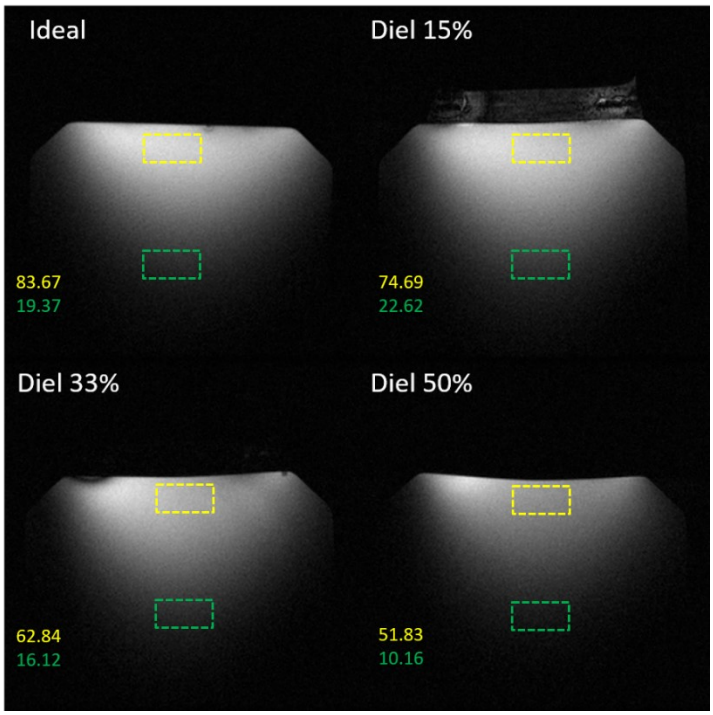


Figure 27. MRI Images Result of Dielectric-loaded Coils

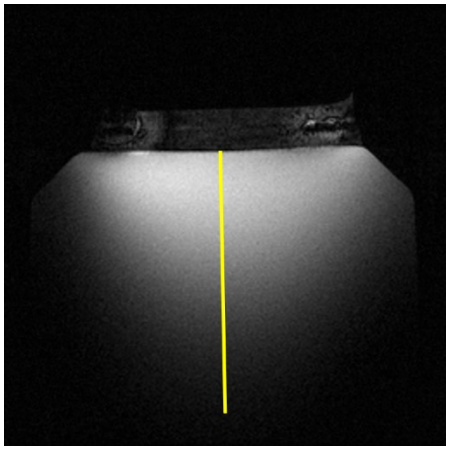

Figure 28. Cut Line Location

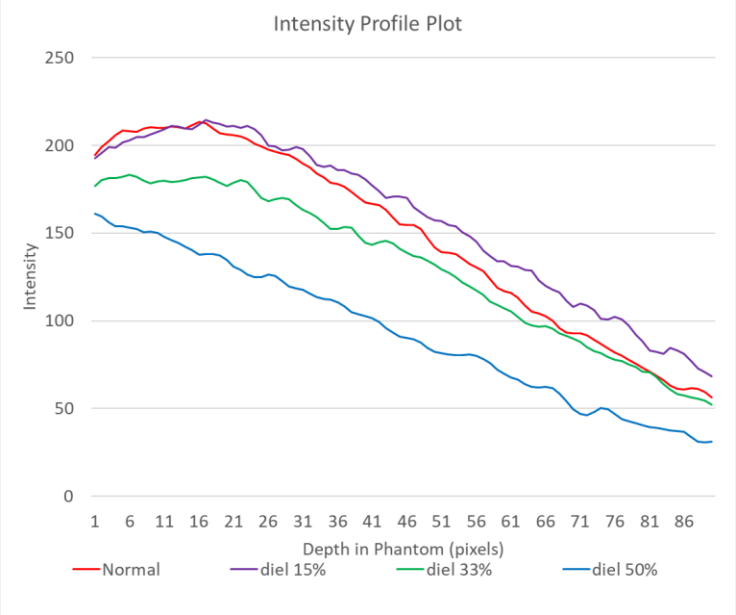


Figure 29. Intensity Profile Comparison Plot

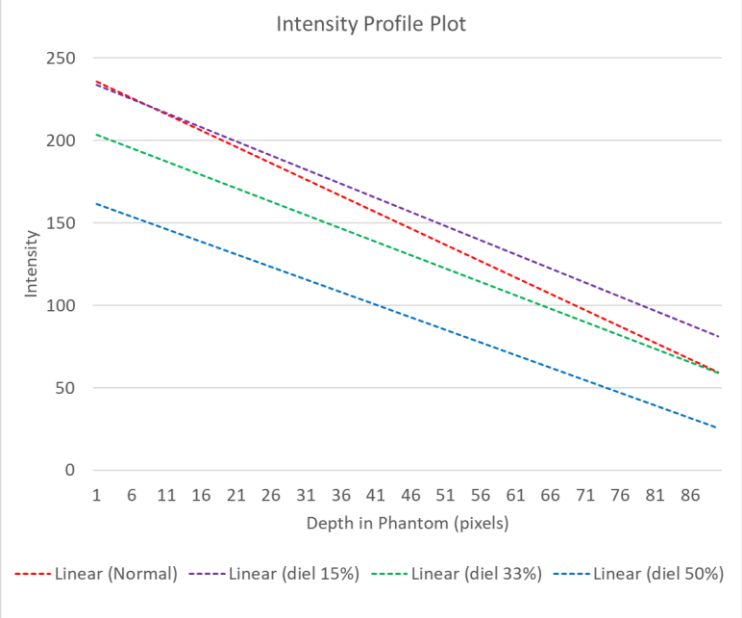


Figure 30. Trend Line of the Intensity Profile Comparison Plot

The SNR of the dielectric integrated coil's upper ROIs are all lower than the ideal coil. As the concentration increases, the SNR decreases. Lower SNR near the surface is not always an undesirable effect. Very high-intensity signals near the surface might saturate the receiver channels, resulting in a lower contrast of the image, which lowers the visibility of the deeper region inside the sample. For the lower ROIs, the SNR of 15% concentration dielectric coil is higher than the ideal. This indicates a higher penetration depth than the ideal coil. However, for the two higher concentrations, the SNR decreases. Trend Line of the Intensity Profile Comparison Plot

A cut line was placed on the phantom to analyze the field's homogeneity, as shown as a yellow line in Figure 28. The intensity profile was plotted along the line of each image and compared in Figure 29. The x-axis of the plot indicates the phantom depth in pixels starting from the surface. The y-axis is the intensity of the image with an intensity resolution of 256. The plot's high-intensity area corresponds to the image's white area. The red line is the intensity profile along the cutline of the ideal coil. The 15% dielectric line shows a similar level of intensity near the surface. The signal intensity also decreases slowly deeper inside the phantom, resulting in the highest penetration depth, which agrees with the SNR analysis. The 33% dielectric coil line has lower intensity near the surface but maintains the same penetration depth as the ideal coil. The dielectric coil with 50% concentration shows the worst intensity.

The overall homogeneity of the field can be approximated with a simple trend line plotted in Figure 30. The slope of the trend line can approximate the homogeneity of the field. The ideal coil has the highest slope steepness of -1.98, while all three dielectric

integrated coils appear to have lower slope steepness. Dielectric integrated coil with concentrations of 15%, 33%, and 50% have slopes of -1.72, -1.62, and -1.53, which are almost similar. This indicates that the dielectric material can improve the homogeneity of the coil's magnetic field.

This experiment shows that the low-concentration dielectric coil is the best option due to the highest penetration depth and good homogeneity. However, the dielectric material surrounding the coil is visible in the image, which is an undesirable effect. Too high concentrations decrease the SNR and degrade the magnetic field. Thus, an optimal value that could yield the best performance might be around 20%. Unfortunately, due to the time limitation, the 33% concentration was selected for further study in this research.

# CHAPTER 8

# STRETCHABLE AND FLEXIBLE DIELECTRIC INTEGRATED RF COIL

## 8.1 Fabrication

The stretchable dielectric integrated coil utilizes the stretchable conductor RF coil embedded inside the dielectric elastomer. The stretchable conductive coil fabricated in Chapter 6 was duplicated. The coil was fixed to a 3D-printed mold and adjusted to be in the middle of the mold, as shown in Figure 31. Then, the dielectric mixture of a medium dielectric concentration of 33%, the most optimal concentration from the previous chapter, was poured into the mold. The mold was put in the vacuum tank to minimize the air bubbles and waited to be cured.

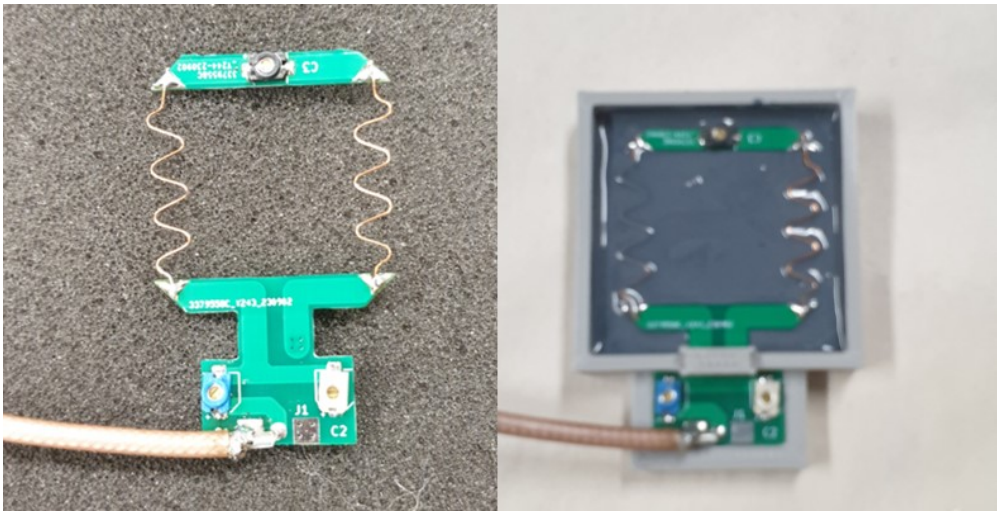


Figure 31. Stretchable RF Coil Fabrication Process

The coil stretcher (Figure 32) was designed to stretch and wrap the coil around a cylindrical phantom to test the coil with the phantom reliably. The level of stretchability is adjustable using the teeth mechanism. Each tooth stretches the coil by 10% in length. This allows the control of the stretching distance at most 20%. Thus, the coil can easily grip the

stretcher and adjust the distance reliably. The mechanical stretchability was tested with the stretcher, as shown in Figure 33 below.

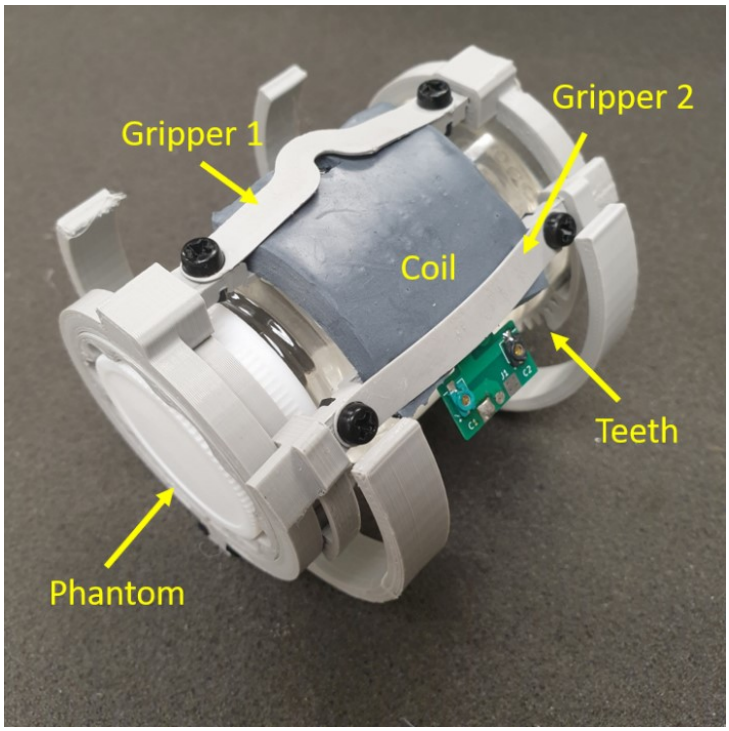


Figure 32. Coil Stretcher Components

Figure 33. The Stretchable Dielectric Integrated RF Coil on the Stretcher

Bench testing with VNA shows a lower resonance frequency after being stretched. This is due to the change in the stretchable conductive components' electrical properties: length and shape. The coil's length also increases, resulting in the coil's overall area increasing. However, the designed matching network can recover the resonance frequency to 400MHz.

## 8.2 Image Acquisition

The dielectric integrated stretchable coils set was tested and compared with the ideal and stretchable coils set. The previous chapter acquired nine images from each coil with the scanner and protocol. The tuning and shimming process was controlled to keep consistency between images.

The result images are illustrated in Figure 34 below. The top row images are the ideal coils set. The middle row images are the stretchable coils set. These two rows are the same images from section 6.3 for comparison purposes. The bottom row images are the stretchable dielectric integrated RF coil stretched to 0%, 10%, and 20% from left to right. 2 ROIs were placed near the surface and deep in the phantom to analyze the SNR.

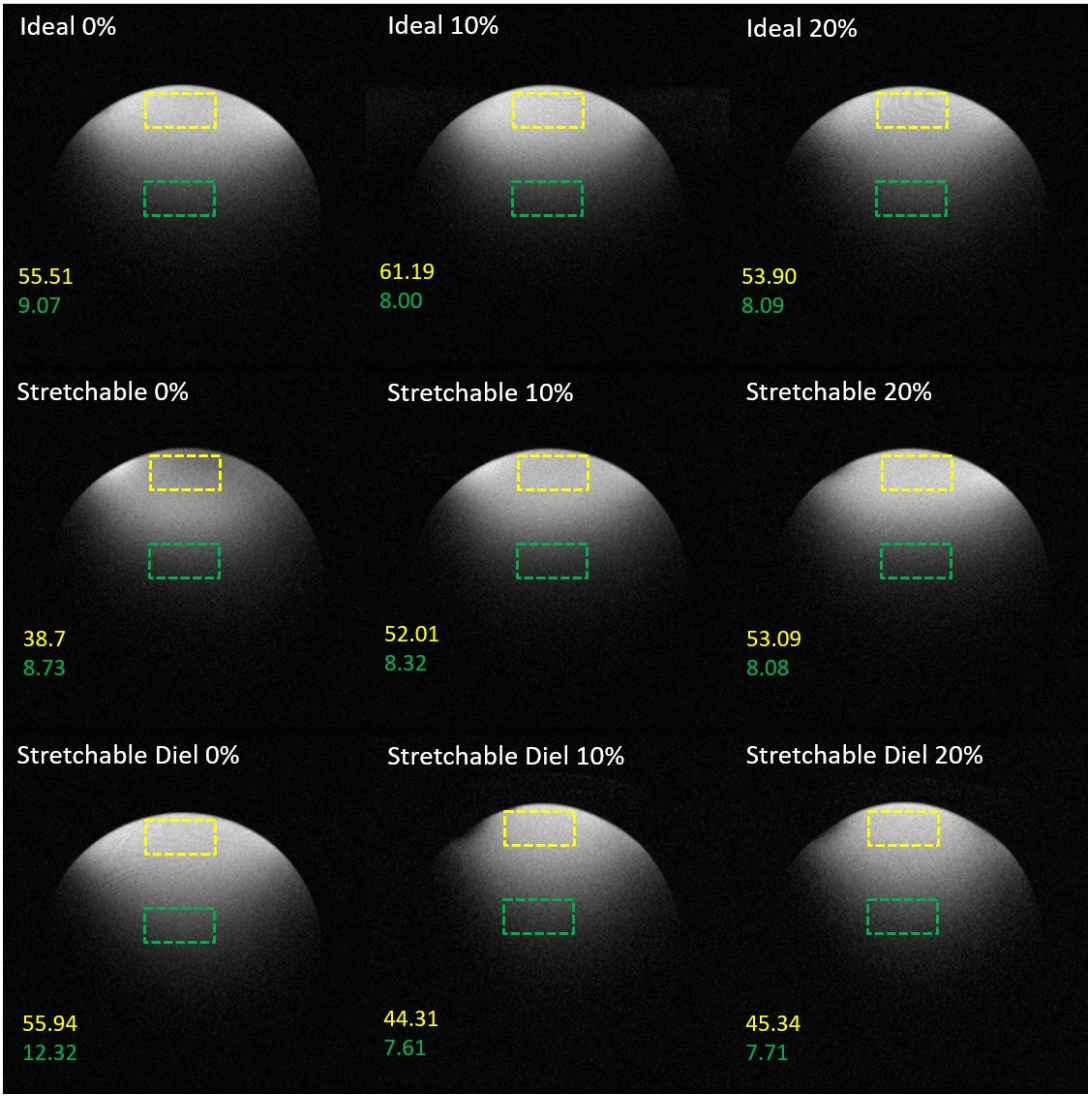


Figure 34. MRI Images Result of Stretchable Dielectric Loaded Coils

By comparing all coil images at 0% stretching distances or the first column, the stretchable coil shows field degradation compared to the ideal coil, as discussed in section 6.3. However, the stretchable dielectric integrated coil has increased SNRs in both upper and lower ROIs. This indicates that the addition of optimized dielectric material can generate the secondary magnetic field to compensate for the stretchable coil's degradation and increase the field's penetration depth. When the coil was stretched to 10%, the degradation effect of the stretchable conductor reduced, resulting in the SNR near the surface starting to return. However, the dielectric coil shows a reduction of the SNR. Compared to both ideal and stretchable coils. The behavior is also similar at 20% stretching. The degradation of the stretchable conductor is minimized since the SNR near the surface of the stretchable coil and the ideal coil are at a similar level. The stretchable dielectric coil also shows a reduction of SNR for both ROIs.

The reduction of the SNR when the coil was stretched shows the result of integrated dielectric material since the stretchable coil set has better SNR when stretched. This reduction might cause a change in the geometry of the dielectric material. When stretched, the flexible material's thickness and width decreased significantly. The distance between the dielectric power particles is also increased. The changes are theorized to severely change the secondary field pattern, which might degrade the overall field, resulting in SNR decreases for both ROIs. To fully understand this behavior, further study must be done. Unfortunately, the investigation of the phenomena is out of the scope of this research.

Even though the flexible and stretchable dielectric integrated coil has comparable or even inferior performance compared to the ideal coil, one has to keep in mind that the ideal coil has the best conductors and filling factor at all stretching lengths, which is not possible for the rigid coil in a practical environment. The proposed coil still excels in flexibility and stretchability, which can increase the filling factor tremendously. Increasing the filling factor is well known to increase the SNR significantly.

# CHAPTER 9

## DISCUSSION AND CONCLUSION

In the early research phase, the RF coils were designed and optimized with EM simulation, bench testing, and imaging with the scanner. Next, the stretchable conductors were fabricated and studied. The components show increases in inductance when being stretched. When corporate with the RF coil, it lowers the resonance frequency. This result agreed with the previous study's simulation and adaptive coil. In imaging results, the stretching component also causes field degradation near the phantom surface. This effect is reduced when the coil is stretched but is still more significant than the ideal coil. The degradation is expected and can potentially be improved by the dielectric material. The stretchable conductor also lowers the penetration depth, which was predicted by the simulation and agreed with the literature. After that, the flexible dielectric material was fabricated and tested. The material provides high flexibility and stretchability. Different concentrations of the dielectric material were made and incorporated with the coils. Testing the coil with VNA shows that the resonance frequency of the dielectric integrated coil shifts lower with high concentration. The material also gets stiffer and less stretchable. Imaging shows that a 15% dielectric powder concentration is insufficient to make the coil invisible. This concentration has the best penetration depth and homogeneity. However, too high a concentration reduces the field's penetration depth and increases the image's background noise. This might be caused by the dielectric coupling between the coil and the dielectric material increasing the coil's Q value. This increment widens the bandwidth of the coil and makes it more susceptible to the coil thermal noise. Thus, the optimal value for dielectric

material was selected at 33% to fabricate the stretchable dielectric integrated coil. Testing the fabricated coil with VNA, the dielectric effect and the stretchable component significantly lower the resonance frequency. When the coil was stretched, the resonance frequency shifted lower. Due to the ideal RF coil geometry design that plans to compensate for these factors, the coil is still in the tunable range. Imaging shows higher SNR when the coil is not stretched. However, the SNRs slightly reduce as the coil is stretched. The change of shape of the dielectric material might be the cause. However, compared to the rigid coil, the flexible and stretchable coil still has advantages in improving the filling factor, which results in better SNR.

To conclude, this work proposed an RF coil integrated with stretchable conductors embedded in flexible elastic dielectric material. The coil is highly flexible and has a stretchability of 20% of its original length. Bench testing and MRI scanning show that the coil performs comparable to the ideal coil sets regarding SNR, field homogeneity, and penetration depth. The elastic dielectric material still had many limitations when this research was conducted. However, it has the potential to be improved in the future, which might increase the performance of the proposed coil.

In further work, multiple channels could be included as a coil array to amplify the stretchability and make the design more practical. With the multi-channel, the coil array can be wrapped around a patient's limb for more clinical use. Furthermore, due to the nature of flexible and stretchable coil, the coil's impedance constantly changes. Automatic tuning and matching can be added to the system to make the coil more convenient.

REFERENCES


1 *Coil Development Calculator - Single Loop Resonator Surface Coil*. (n.d.). Retrieved November 12, 2023, from https://bio.groups.et.byu.net/CoilDevCal.phtml

2 Gruber, B., Froeling, M., Leiner, T., & Klomp, D. W. J. (2018). RF coils: A practical guide for nonphysicists. *Journal of Magnetic Resonance Imaging*, *48*(3), 590–604. https://doi.org/10.1002/JMRI.26187

3 Gruber, B., Rehner, R., Laistler, E., & Zink, S. (2020). Anatomically Adaptive Coils for MRI—A 6-Channel Array for Knee Imaging at 1.5 Tesla. *Frontiers in Physics*, *8*, 516087. https://doi.org/10.3389/FPHY.2020.00080/BIBTEX

4 *Gyromagnetic ratio (γ) - Questions and Answers in MRI*. (n.d.). Retrieved November 12, 2023, from https://mriquestions.com/gyromagnetic-ratio-gamma.html

5 Hashemi, S., Kandala, S. K., Agbo, B., Colwell, Z. A., Song, K., Xie, R., & Sohn, S.-M. (2023). Flexible, Stretchable, and MR-Invisible Dielectric Material for Magnetic Resonance Imaging. *IEEE Journal of Electromagnetics, RF and Microwaves in Medicine and Biology*, 1–8. https://doi.org/10.1109/JERM.2023.3321873

6 Hashemi, S., Kandala, S. K., & Sohn, S. M. (2023). Dielectric Loaded decoupling technique for multichannel RF coils. *IEEE MTT-S International Microwave Symposium Digest*, *2023-June*, 779–782. https://doi.org/10.1109/IMS37964.2023.10188149

7 *Inductance of Rectangular Loop · Technick.net*. (n.d.). Retrieved November 12, 2023, from https://technick.net/tools/inductance-calculator/rectangular-loop/

8 Lakshmanan, K., Carluccio, G., Walczyk, J., Brown, R., Rupprecht, S., Yang, Q. X., Lanagan, M. T., & Collins, C. M. (2021). Improved whole-brain SNR with an integrated high-permittivity material in a head array at 7T. *Magnetic Resonance in Medicine*, *86*(2), 1167–1174. https://doi.org/10.1002/MRM.28780

9 *Larmor frequency - Questions and Answers in MRI*. (n.d.). Retrieved November 12, 2023, from https://mriquestions.com/who-was-larmor.html

10 *Nuclear precession - Questions and Answers in MRI*. (n.d.). Retrieved November 12, 2023, from https://mriquestions.com/why-precession.html

11 Ruello, G., & Lattanzi, R. (2022). A Physical Framework to Interpret the Effects of High Permittivity Materials on Radiofrequency Coil Performance in Magnetic Resonance Imaging. *IEEE Transactions on Biomedical Engineering*, *69*(11), 3278–3287. https://doi.org/10.1109/TBME.2022.3165763

12 Ruytenberg, T., O'Reilly, T. P., & Webb, A. G. (2020). Design and characterization of receive-only surface coil arrays at 3T with integrated solid high permittivity materials. *Journal of Magnetic Resonance*, *311*, 106681. https://doi.org/10.1016/J.JMR.2019.106681

13 *Spin - Questions and Answers in MRI*. (n.d.). Retrieved November 12, 2023, from https://mriquestions.com/what-is-spin.html

14 Webb, A. G. (2011). Dielectric materials in magnetic resonance. *Concepts in Magnetic Resonance Part A*, *38A*(4), 148–184. https://doi.org/10.1002/CMR.A.20219

15 Yang, Q. X., Mao, W., Wang, J., Smith, M. B., Lei, H., Zhang, X., Ugurbil, K., & Chen, W. (2006). Manipulation of image intensity distribution at 7.0 T: passive RF shimming and focusing with dielectric materials. *Journal of Magnetic Resonance Imaging : JMRI*, *24*(1), 197–202. https://doi.org/10.1002/JMRI.20603

16 Yang, Q. X., Wang, J., Wang, J., Collins, C. M., Wang, C., & Smith, M. B. (2011). Reducing SAR and Enhancing Cerebral Signal-to-Noise Ratio with High Permittivity Padding at 3 T. *Magn Reson Med*, *65*(2), 358–362. https://doi.org/10.1002/mrm.22695